Spectrochimica Acta Part A 82 (2011) 8–19

Contents lists available at ScienceDirect

Spectrochimica Acta Part A: Molecular and Biomolecular Spectroscopy

journal homepage: www.elsevier.com/locate/saa

Ligational behaviour of lomefloxacin drug towards Cr(III), Mn(II), Fe(III), Co(II), Ni(II), Cu(II), Zn(II), Th(IV) and UO_2(VI) ions: Synthesis, structural characterization and biological activity studies

Hanan F. Abd El-Halim [a], Gehad G. Mohamed [b,*], Maher M.I. El-Dessouky [a], Walaa H. Mahmoud [b]

[a] Pharmaceutical Chemistry Department, Faculty of Pharmacy, Misr International University, Cairo, Egypt
[b] Chemistry Department, Faculty of Science, Cairo University, 12613, Giza, Egypt

ARTICLE INFO

Article history:
Received 13 April 2011
Received in revised form 19 May 2011
Accepted 25 May 2011

Keywords:
Lomefloxacin
Metal complexes
Spectroscopy
Thermal analyses
Biological activity
Anticancer activity

ABSTRACT

Nine new mononuclear Cr(III), Mn(II), Fe(III), Co(II), Ni(II), Cu(II), Zn(II), Th(IV) and UO_2(VI) complexes of lomefloxacin drug were synthesized. The structures of these complexes were elucidated by elemental analyses, IR, XRD, UV–vis, ^{1}H NMR as well as conductivity and magnetic susceptibility measurements and thermal analyses. The dissociation constants of lomefloxacin and stability constants of its binary complexes have been determined spectrophotometrically in aqueous solution at 25 ± 1 °C and at 0.1 M KNO_3 ionic strength. The discussion of the outcome data of the prepared complexes indicate that the lomefloxacin ligand behaves as a neutral bidentate ligand through OO coordination sites and coordinated to the metal ions via the carbonyl oxygen and protonated carboxylic oxygen with 1:1 (metal:ligand) stoichiometry for all complexes. The molar conductance measurements proved that the complexes are electrolytes. The powder XRD study reflects the crystalline nature for the investigated ligand and its complexes except Mn(II), Zn(II) and UO_2(II). The geometrical structures of these complexes are found to be octahedral. The thermal behaviour of these chelates is studied where the hydrated complexes lose water molecules of hydration in the first steps followed by decomposition of the anions, coordinated water and ligand molecules in the subsequent steps. The activation thermodynamic parameters are calculated using Coats–Redfern and Horowitz–Metzger methods. A comparative study of the inhibition zones of the ligand and its metal complexes indicates that metal complexes exhibit higher antibacterial effect against one or more bacterial species than the free LFX ligand. The antifungal and anticancer activities were also tested. The antifungal effect of almost metal complexes is higher than the free ligand. LFX, $[Co(LFX)(H_2O)_4]\cdot Cl_2$ and $[Zn(LFX)(H_2O)_4]\cdot Cl_2$ were found to be very active with IC50 values 14, 11.2 and 43.1, respectively. While, other complexes had been found to be inactive at lower concentration than 100 μg/ml.

1. Introduction

Lomefloxacin is a bactericidal fluoroquinolone agent with activity against a wide range of gram-negative and gram-positive organisms. Its IUPAC name is 1-ethyl-6,8-difluoro-7-(3-methylpiperazin-1-yl)-4-oxoquinoline-3-carboxylic acid (Fig. 1). The bactericidal action of lomefloxacin resulted from interference with the activity of the bacterial enzymes DNA gyrase and topoisomerase IV, which are needed for the transcription and replication of bacterial DNA [1]. Modifications of LFX were made based on structure–activity relationships. It was discovered that a fluorine atom at position 6 and a piperazine ring at position 7 greatly enhance the spectrum of activity. Recently, a relatively new approach to the rational design of antitumor agents has been introduced based on some new quinolone molecules that display a novel mode of action [2,3].

The fluoroquinolones constitute an important class of synthetic antimicrobial agents which have been the subject of intensive study [4]. They possess a broad spectrum of activity against various pathogenic microorganisms, and resistant to aminoglycosides, penicillins, cephalosporins, tetracyclines and other antibiotics. This class of compounds, when compared to existing bactericidal drugs, shows improved pharmacokinetic properties and a broad spectrum of activity against parasites, bacteria, and mycobacteria, including resistant strains [5,6]. Metal coordination to biologically active molecules can be used as a strategy to enhance their activity and overcome resistance. Quinolones are particularly interesting due to their ability to coordinate metal ions. Thus, numerous studies regarding the interaction between quinolones with metallic cations have been reported in the literature [2,7–9]. Some of these metal complexes have been tested successfully for antibacterial activity [10–15]. The effect of metal ions on the antibacterial activity of

* Corresponding author. Tel.: +20 1523423103; fax: +20 235728843.
E-mail address: ggenidy@hotmail.com (G.G. Mohamed).

1386-1425/$ – see front matter © 2011 Elsevier B.V. All rights reserved.
doi:10.1016/j.saa.2011.05.089

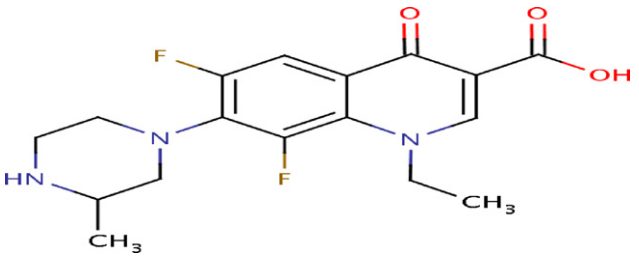

Fig. 1. Structural formula of lomefloxacin drug.

norfloxacin has been previously reported. Fe(III) and Zn(II) complexes were obtained and they showed increased activity over norfloxacin against Gram negative *E. coli* and *Bacillus dysenteriae* [16]. Jain et al. [17] have reported a Co(II) complex with sparfloxacin which is more potent against several pathogenic bacteria than sparfloxacin. In a similar approach, Saha et al. [18] showed that the Cu(II) complex and ciprofloxacin presents a significant enhancement in antitubercular activity. Usually the fluoroquinolones act as bidentate ligands binding to the metal ions through the carboxylate and carbonyl oxygens. The metal ions can form a stable 6-member chelate ring with a slightly distorted octahedral geometry as was observed for Co(II), Ni(II), Zn(II), Cd(II), Mn(II) and Cu(II) complexes [13,19–21]. This site seems to be preferred for most metal ions. Coordination of the fluoroquinolones with metal ions by way of the piperazine nitrogen atoms is much less common [22].

As part of our ongoing study of metal complexes of fluoroquinolones [23,24], we report herein the coordination chemistry and bioactivity of some transition metal complexes containing oxygen–oxygen donor sites. The aim of the current work is to study the chelating behaviour of LFX drug towards some transition metals. The structures of the metal complexes were characterized by elemental analyses, IR, ^{1}H NMR, UV–vis, XRD, conductivity and magnetic susceptibility measurements at room temperature, thermal analyses as well as some results of bioactivity tests are also included.

2. Experimental

2.1. Material and reagent

All chemicals used were of the analytical reagent grade (AR), and of highest purity available. They included lomefloxacine drug, $CuCl_2{\cdot}2H_2O$, $MnCl_2{\cdot}2H_2O$, $CrCl_3{\cdot}6H_2O$ and $UO_2(NO_3)_2{\cdot}2H_2O$ (Sigma), $CoCl_2{\cdot}6H_2O$ and $NiCl_2{\cdot}6H_2O$ (BDH), $ThCl_4$ (Aldrich), $ZnCl_2{\cdot}2H_2O$ (Ubichem) and $FeCl_3{\cdot}6H_2O$ (Prolabo). Organic solvents were spectroscopic pure from BDH included ethanol, diethyl ether and dimethylformamide. Hydrogen peroxide and sodium chloride, sodium carbonate and sodium hydroxide (A.R.) were used. Hydrochloric, phosphoric, acetic, boric and nitric acids (Merck) were used.

Human tumor cell lines (Brest cell) were obtained frozen in liquid nitrogen (−180 °C) from the American Type Culture Collection. The tumor cell lines were maintained in the National Cancer Institute, Cairo, Egypt, by serial sub-culturing.

2.2. Solutions

A fresh stock solution of 1×10^{-3} M of LFX (0.351 g/L) was prepared by dissolving the accurately weighed amount in the appropriate volume of absolute ethanol. 1×10^{-3} M Stock solutions of the metal salts (Fe(III), 0.27 g/L; Co(II), 0.23 g/L; Ni(II), 0.23 g/L; Cu(II), 0.17 g/L; Zn(II), 0.172 g/L; Cr(III), 0.26 g/L; UO_2(II), 0.50 g/L, Mn(II), 0.16 g/L and Th(IV), 0.37 g/L) were prepared by dissolving the accurately weighed amounts of the metal salts in the appropriate volume of de-ionized water. Acid mixture (0.04 M phosphoric, acetic and boric acids) from which series of universal buffer solutions of different pH values (2–12) were prepared by using 0.1 N sodium hydroxide solution for adjusting the desired pH.

Dimethylsulphoxide (DMSO) (Sigma Chemical Co., St. Louis, MO, and U.S.A.): It was used in cryopreservation of cells. RPMI-1640 medium (Sigma Chemical Co., St. Louis, MO, and U.S.A.). The medium was used for culturing and maintenance of the human tumor cell lines. The medium was supplied in a powder form. It was prepared as follows: 10.4 g medium was weighed, mixed with 2 g sodium bicarbonate, completed to 1 L with distilled water and shacked carefully till complete dissolution. The medium was then sterilized by filtration in a Millipore bacterial filter (0.22 μm). The prepared medium was kept in a refrigerator (4 °C) and checked at regular intervals for contamination. Before use, the medium was warmed at 37 °C in a water bath and the supplemented with penicillin/streptomycin and FBS.

Sodium bicarbonate (Sigma Chemical Co., St. Louis, MO, U.S.A.) was used for the preparation of RPMI-1640 medium. 0.05% isotonic Trypan blue solution (Sigma Chemical Co., St. Louis, MO, U.S.A.) was prepared in normal saline and was used for viability counting. 10% Fetal Bovine Serum (FBS) (heat inactivated at 56 °C for 30 min), 100 units/ml Penicillin and 2 mg/ml Streptomycin were supplied from Sigma Chemical Co., St. Louis, MO, U.S.A. and were used for the supplementation of RPMI-1640 medium prior to use. 0.025% (w/v) Trypsin (Sigma Chemical Co., St. Louis, MO, U.S.A.) was used for the harvesting of cells. 1% (v/v) Acetic acid (Sigma Chemical Co., St. Louis, MO, U.S.A.) was used for dissolving the unbound SRB dye. 0.4% Sulphorhodamine-B (SRB) (Sigma Chemical Co., St. Louis, MO, U.S.A.) dissolved in 1% acetic acid was used as a protein dye. A stock solution of trichloroacetic acid (TCA, 50%, Sigma Chemical Co., St. Louis, MO, U.S.A.) was prepared and stored. 50 μl of the stock was added to 200 μl RPMI-1640 medium/well to yield a final concentration of 10% used for protein precipitation. 100% isopropanol and 70% ethanol were used. Tris base 10 mM (pH 10.5) was used for SRB dye solubilization. 121.1 g of tris base was dissolved in 1000 ml of distilled water and pH was adjusted by HCl acid (2 M).

2.3. Measurements

Microanalyses of carbon, hydrogen and nitrogen were carried out at the Microanalytical Center, Cairo University, Egypt, using CHNS-932 (LECO) Vario Elemental Analyzer. Analyses of the metal content were followed by the dissolution of the solid complexes in concentrated HNO_3, neutralizing the diluted aqueous solutions with ammonia and titrating the metal solutions with EDTA. pH measurements were carried out using Jenway 3505 pH meter, U.K. FT-IR spectra were recorded on a Perkin-Elmer 1650 spectrometer (4000–400 cm^{-1}) in KBr pellets. Electronic spectra (measured in ethanol) and diffused reflectance spectra (measured as $BaSO_4$ disc) were recorded at room temperature on a Shimadzu 3101pc spectrophotometer. ^{1}H NMR spectra, as a solution in DMSO-*d6*, were recorded on a 300 MHz Varian-Oxford Mercury at room temperature using TMS as an internal standard. Mass spectra were recorded by the EI technique at 70 eV using MS-5988 GS–MS Hewlett-Packard instrument at the Microanalytical Center, Cairo University. The molar magnetic susceptibility was measured on powdered samples using the Faraday method. The diamagnetic corrections were made by Pascal's constant and $Hg[Co(SCN)_4]$ was used as a calibrant. Molar conductivities of 10^{-3} M solutions of the solid complexes in DMF were measured using Jenway 4010 conductivity meter. The thermogravimetric analyses (TG, DTG and DTA) of the solid complexes were carried out from room temperature to 800 °C using a Shimadzu TG-50H thermal analyzer. The X-ray powder diffraction analyses were carried out using Philips Analytical X-Ray BV, diffractometer type PW 1840. Radiation was provided by cop-

per target (Cu anode 2000 W) high intensity X-ray tube operated at 40 kV and 25 mA. Divergence and the receiving slits were 1 and 0.2, respectively. The antibacterial and antifungal activities were evaluated at the Microbiological laboratory, Microanalytical center, Cairo University, Egypt. The anticancer activity was performed at the National Cancer Institute, Cancer Biology Department, Pharmacology Department, Cairo University. The optical density (O.D.) of each well was measured spectrophotometrically at 564 nm with an ELIZA microplate reader (Meter tech. Σ 960, U.S.A.).

2.4. Synthesis of metal complexes

Ethanolic or aqueous-ethanolic solution of lomefloxacin (0.4 g, 1.03 mmol) and hydrated metal salts (0.274 g Cr(III), 0.167 g Mn(II), 0.278 g Fe(III), 0.244 g Co(II), 0.244 g Ni(II), 0.176 g Cu(II), 0.176 g Zn(II), 0.385 g Th(IV) and 0.517 g UO_2(II), 1.0 mmol) were heated under reflux for 2–3 h. The precipitates were filtered off, washed with ethanol followed by diethyl ether and dried in vacuum desiccator over anhydrous $CaCl_2$. The physical and analytical data of the isolated complexes are listed in Suppl. Table 1. The complexes have high melting points and insoluble in common organic solvents and soluble in DMF or DMSO.

2.5. Spectrophotometric studies

The absorption spectra of the LFX free ligand and its binary complexes under study were scanned within the wavelength range from 200 to 600 nm. The absorption spectra of 1×10^{-3} M solution of this ligand and its complexes were measured in a universal buffer of different pH values ranged from 2 to 12. Two methods were applied for the determination of pK_a values of free ligand namely half height and limiting absorbance methods [25].

2.6. Biological activity

A filter paper disk (5 mm) was transferred into 250 ml flasks containing 20 ml of working volume of tested solution (100 g/ml). All flasks were autoclaved for 20 min at 121 °C. LB agar media surfaces were inoculated with two investigated bacteria (gram positive and gram negative) and two strains of fungi then, transferred to a saturated disk with a tested solution in the center of Petri dish (agar plates). Finally, all these Petri dishes were incubated at 25 °C for 48 h where clear or inhibition zones were detected around each disk. Control flask of the experiment was designed to perform under the same condition described previously for each microorganism but with dimethylformamide solution only and by subtracting the diameter of inhibition zone resulting with dimethylformamide from that obtained in each case, so antibacterial activity could be calculated [26]. All experiments were performed as triplicate and data plotted were the mean value.

2.7. Anticancer activity

Potential cytotoxicity of the compounds was tested using the method of Skehan et al. [27]. Cells were plated in 96-multiwell plate (104 cells/well) for 24 h before treatment with the compounds to allow attachment of cell to the wall of the plate. Different concentrations of the compounds under investigation (0, 5, 12.5, 25, 50 and 100 μg/ml) were added to the cell monolayer triplicate wells were prepared for each individual dose. The monolayer cells were incubated with the compounds for 48 h at 37 °C and in 5% CO_2 atmosphere. After 48 h, cells were fixed, washed and stained with SRB stain. Excess stain was washed with acetic acid and attached stain was recovered with tris-EDTA buffer. The optical density (O.D.) of each well was measured spectrophotometrically at 564 nm with an ELIZA microplate reader and the mean background absorbance was automatically subtracted and mean values of each drug concentration was calculated. The relation between surviving fraction and drug concentration is plotted to get the survival curve of Breath tumor cell line for each compound.

Calculation: The percentage of cell survival was calculated as follows:

$$\text{survival fraction} = \frac{\text{O.D.(treated cells)}}{\text{O.D.(control cells)}}.$$

The IC_{50} values (the concentrations of thymoquinone required to produce 50% inhibition of cell growth). The experiment was repeated 3 times for each cell line.

3. Results and discussion

3.1. Mass spectrum of LFX

The electron impact mass spectrum of LFX is recorded and investigated at 70 eV of electron energy. The mass spectrum of the studied drug is characterized by moderate to high intensity molecular ion peaks at 70 eV. The abundance of the molecular ion depends mainly on the structure (and therefore the potential energy surface) of the molecular ion. The mass spectrum of LFX shows a well-defined parent peak at $m/z = 351$ (M^+) with a relative intensity = 29%. The parent ion and the fragments obtained by cleavage in different positions in LFX molecule are shown in Scheme 1.

3.2. Dissociation constants of LFX

Lomefloxacin drug is considered as quinoline derivatives which derived from nalidixic acid. Nalidixic acid has a single protonation constant (pK_a = 6) in the pH range of 2–9 [2,28]. It is protonated in a strong acid solution to form a naphthyridinium cation with a pK_a of −0.86 [29]. The drug exists in its undissociated form over the pH range of 1.6–3.6. Fluoroquinolone analogues with the piperazinyl group in the 7-position contain two relevant ionizable functional groups. The protolytic equilibria of lomefloxacin are expressed in Scheme 2. This molecule can exist in four possible forms: an acidic cation H_2Q^+, a neutral nonionized species HQ, an intermediate zwitter ion $HQ^{\pm}$ and a basic anion Q^-, depending on the pH. At low pH values, both the 7-piperazinyl group and 3-carboxyl group are protonated, whereas at high pH values, neither is protonated. The carboxyl group is normally a stronger acid than the ammonium group, the reason being that the neutral nonionic form is spontaneously rearranged to the zwitter ion. Two macroscopic dissociation constants can be determined for lomefloxacin. The first (pK_{a1} = 5.57) applies to the 3-carboxyl proton and the second (pK_{a2} = 11.50) to the 7-piperazinyl proton. The decrease in acidity of the carboxylic group compared with benzoic acid (pK_a = 4.2) is explained by the intramolecular hydrogen bond to the keto oxygen [2,30]. The pK_{a2}, which is due to the presence of an ionizable proton on the external piperazinyl nitrogen, was found at around 11.5.

3.3. UV–vis spectra of metal chelates

UV–visible spectral data of the free LFX ligand and its binary chelates (1×10^{-3} M) solutions in aqueous universal buffer of varying pH values from 2 to 12 at λ ranging from 200 to 600 nm using the same solvent as blank are studied. In neutral and alkaline medium, free LFX ligand gives two maximum bands, the first at 325 nm and another shoulder band at 295 nm. These bands may be attributed to $n \rightarrow \pi^*$ and $\pi \rightarrow \pi^*$ transitions inside the LFX molecule. While, in acidic medium the $n \rightarrow \pi^*$ transition may be disappear due to the protonation of nitrogen atom.

It is obvious that the absorption spectra of the binary complexes have the same behaviour like the free LFX ligand. The band at

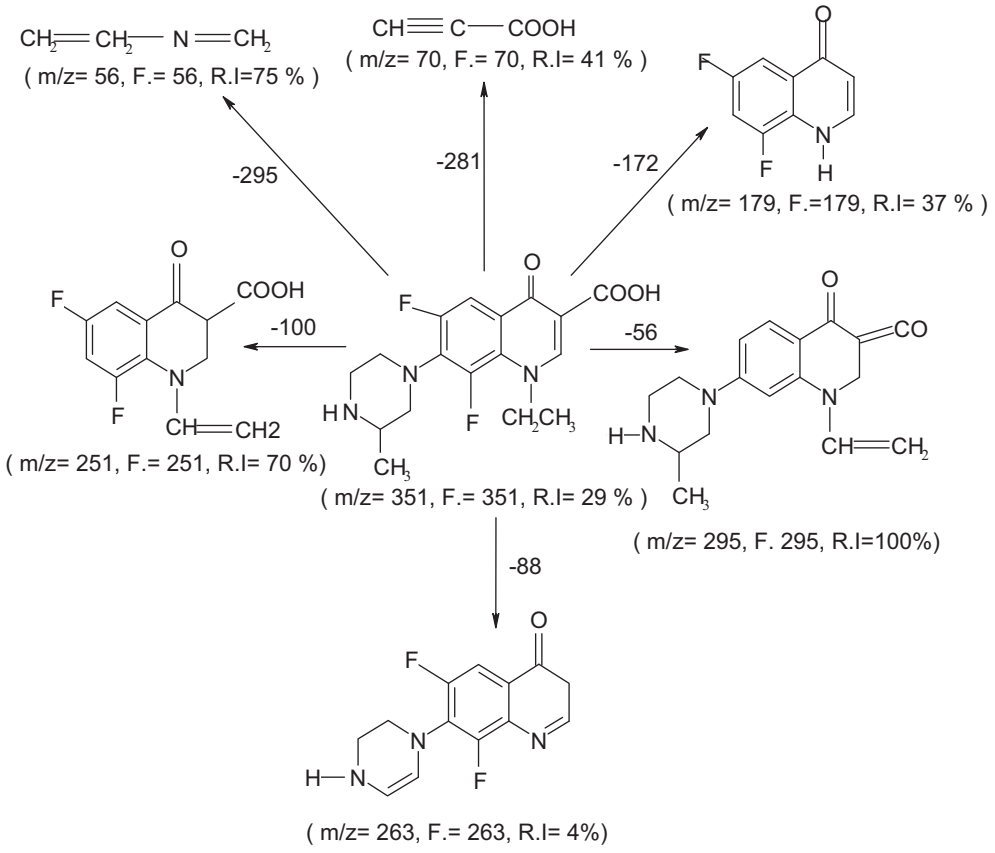

Scheme 1. Mass fragmentation pattern of LFX.

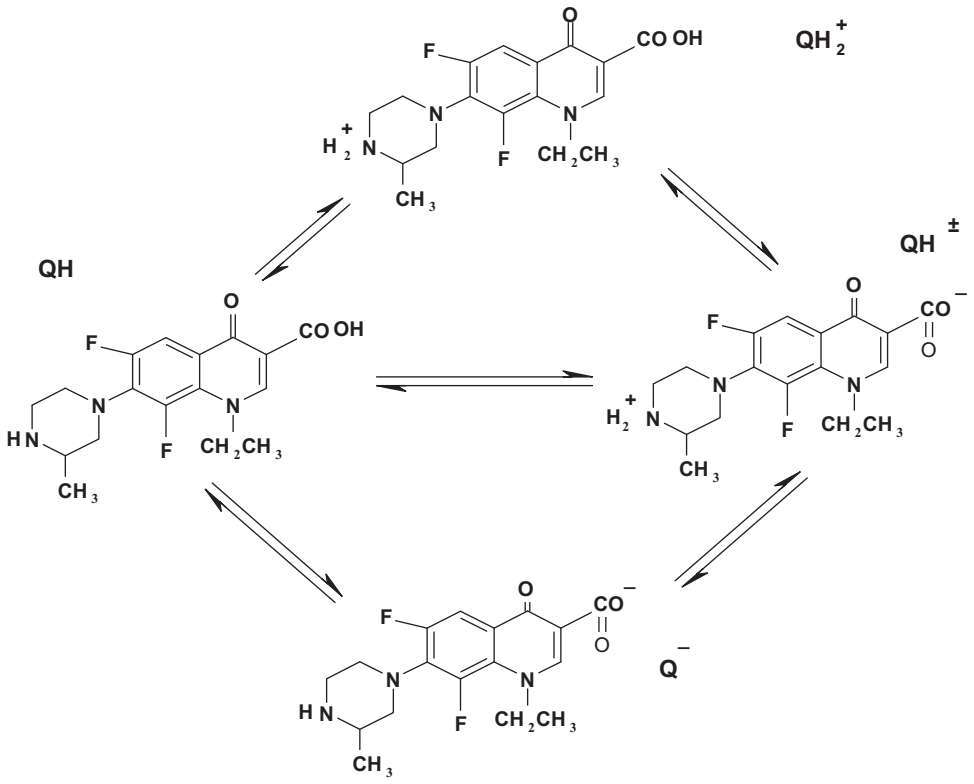

Scheme 2. Protolytic equilibria in lomefloxacin drug water solutions.

320 nm may be assigned to $n \rightarrow \pi^*$ transition within the C=O group or carboxylate group of free LFX ligand. This band is red shifted to 321–326 nm in Cr(III), Th(IV) and UO_2(II) chelates, while it disappeared in all the remaining chelates revealing the involvement of the C=O group and carboxylate–O in chelate formation [28,31].

3.4. Calculation of the metal complexes formation constants

The stability constants are obtained spectrophotometrically [32,33] by measuring the absorbance of solutions of LFX ligand and metal at fixed concentration but at distinct pH values ranging from 2 to 12. The degree of formation of the complex is obtained from the relationship

$$\tilde{n} = \frac{A_x - A_L}{A_{ML} - A_L} \quad (1)$$

where A_x, A_L and A_{ML} are the absorbances of the partially formed complex at a specific pH, the free LFX ligand and the fully formed complex, respectively. Then, the negative logarithm of the concentration of non-protonated ligand (pL) was obtained using Eq. (2):

$$pL = \log \frac{1 + B_1^H[H^+] + B_2^H[H^+]^2 + \cdots}{T_L - nT_M} \quad (2)$$

where $B_1{}^H$ and $B_2{}^H$ are the reciprocals of the acid dissociation constants of the LFX ligand, i.e. $[LH_1]/[L][H]$ and $[LH_2]/[L][H]^2$, respectively. T_L and T_M represent the stoichiometric concentration of the LFX ligand and metal. The stability constant (K) can be calculated from Eq. (3).

$$\tilde{n} + (\tilde{n} - 1)K(L) = 0 \quad (3)$$

The calculated log K values for the Cr(III), Mn(II), Fe(III), Co(II), Ni(II), Cu(II), Zn(II), Th(IV) and UO_2(II) complexes are given in Suppl. Table 1. It is obvious that the complex-forming abilities of the transition metal ions are frequently characterized by stability orders. The order of stability constants is found to be Cu(II) > Ni(II) > Co(II) > Mn(II) and Cr(III) in accordance with Irving and Williams order [34] for divalent metal ions of the 3d series. It is clear from Suppl. Table 1 that the stability of Cu(II) complex is considerably larger as compared to other metals of the 3rd series. Under the influence of the ligand field, Cu(II)($3d^9$) will receive some extra stabilization [35] due to tetragonal distortion of octahedral symmetry in their complexes. The Cu(II) complex will be further stabilized due to the Jahn–Teller effect [36]. The free energy of formation, ΔG°, accompanying the complexation reaction is found to be from −56.55 to −57.63 kJ mol^{-1} at 25 °C.

From the previous data, it is apparent that the negative values of ΔG° show that the driving tendency of the complexation reaction is from left to right and the reaction proceeds spontaneously.

3.5. Elemental analyses of the complexes

The results of elemental analyses (C, H, and N) with molecular formula and the melting points are presented in Suppl. Table 1. The results obtained are in good agreement with those calculated for the suggested formula, and the melting point is sharp indicating the purity of the prepared metal complexes.

3.6. Molar conductance measurements

The chelates are dissolved in DMF and the molar conductivities of their 10^{-3} M solutions at 25 ± 2 °C are measured. It is concluded from the results given in Suppl. Table 1 that the Fe(III) and Cr(III) chelates have molar conductivity values of 290 and 278 Ω^{-1} mol^{-1} cm^2, respectively, indicating that they are 1:3 electrolytes. The molar conductivity values of Mn(II), Co(II), Ni(II),

Table 1
IR spectra (4000–400 cm^{-1}) of LFX and its binary metal complexes.

LFX	$[Cr(LFX)(H_2O)_4]Cl_3{\cdot}2H_2O$	$[Mn(LFX)(H_2O)_4]Cl_2{\cdot}2H_2O$	$[Fe(LFX)(H_2O)_4]Cl_3{\cdot}2H_2O$	$[Co(LFX)(H_2O)_4]Cl_2{\cdot}2H_2O$	$[Ni(LFX)(H_2O)_4]Cl_2{\cdot}H_2O$	$[Cu(LFX)(H_2O)_4]Cl_2{\cdot}2H_2O$	$[Zn(LFX)(H_2O)_4]Cl_2{\cdot}2H_2O$	$[Th(LFX)(H_2O)_4]Cl_4{\cdot}2H_2O$	$[UO_2(LFX)(NO_3)_2$	Assignment
3367br	3389br	3389br	3389br	3376br	3350br	3389br	3480br	3363br	3360br	OH stretching
2925m	2925s	2925m	2925s	2925m	2948s	2925s	2892s	2856s	2850w	CH stretch in CH_3 and in CH_2 groups
1725sh	1721sh	Dis	Dis	Dis	Dis	Dis	Dis	1739s	1739s	C=O stretch
1615sh	1622m	1618m	1617m	1622s	1617m	1618sh	1615m	1623s	1615s	C=C and C=N stretching
1590m	1528m	1573m	1523sh	1580s	1560m	1591m	1545m	1550m	1530m	COO asym
1473m	1456sh	1482m	1449m	1452s	1476m	1469 m	1475m	1470mm	1450w	CH_2 deformation
1396s	1400m	1392m	1390 m	1402s	1420mm	1405s	1370s	1396s	1382s	COO sym
1258m	1251sh	1255s	1249s	1250 m	1253m	1251m	1252m	1250s	1250s	CH in plane bending
1171w	1171s	1171s	1171s	1171s	1171s	1171s	1171s	1171s	1171s	CH bend + CH twist and C–O stretch
1094m	1092m	1091m	1049sh	1091sh	1091sh	1052sh	1090sh	1050sh	1049s	Benzene ring + pyridine ring stretch
808sh	810sh	816sh	811sh	813sh	812sh	812sh	817sh	812sh	814sh	C–N stretching
650w	650s	657m	650s	650s	659m	650w	659s	658s	658m	C–F stretching
–	552s	540s	550s	549s	540s	545s	535s	530s	534m	M–O stretching
–	454s	498m	458s	490s	470s	470s	490s	406s	460m	M–O stretching of coordinated water

s, small; m, medium; br, broad; sh, sharp; w, weak.

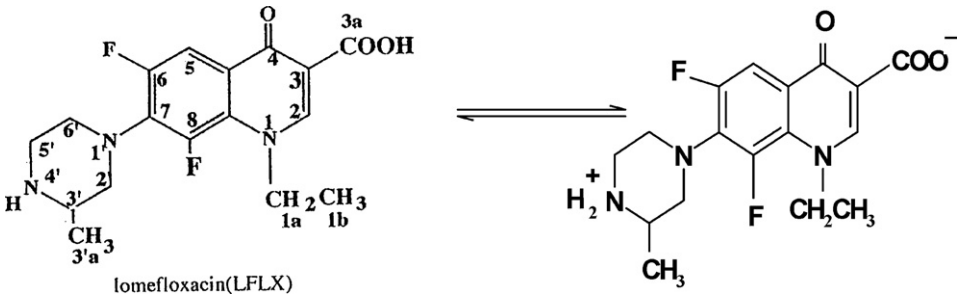

Scheme 3. Zwitter-ion formation of LFX.

Cu(II), Zn(II) and UO_2(II) chelates under investigation (Suppl. Table 1) are found to be 165, 159, 136, 115, 176 and 146 Ω^{-1} mol^{-1} cm^2, respectively. It is obvious from these data that these chelates are ionic in nature and they are of the type 1:2 electrolytes. Th(IV) complex has a molar conductance value of 314 Ω^{-1} mol^{-1} cm^2, indicating that it is 1:4 electrolyte.

3.7. Infrared spectra and mode of bonding

In the absence of a powerful technique, such as X-ray crystallography, IR spectra has proven to be the most suitable technique to give enough information to elucidate the way of bonding of LFX to the metal ions. The IR spectra of the free LFX ligand and its metal complexes were carried out in the range of 4000–400 cm^{-1} and the most effective bands are listed in Table 1. The strong band observed at 1725 cm^{-1} in the free LFX ligand is assigned to the carbonyl stretching vibration [37,38]. This band is found in the spectra of the complexes at 1721–1739 cm^{-1} (Table 1) or disappeared in some complexes indicating the participation of carbonyl oxygen atom in coordination (M–O) [38]. The υ(OH), υ_{asym}(COO) and υ_{sym}(COO) stretching vibrations are observed at 3367, 1590 and 1396 cm^{-1}, respectively, for LFX free ligand [23,24,38]. The υ(OH) band is still broad in all complexes, which renders it difficult to attribute to the involvement of OH group in coordination, since, according to the elemental analysis and thermogravimetric studies, most of the complexes obtained contain water of crystallization and coordination. Coordination with metal ions via the carboxylate O atom is indicated by shift in position of υ_{asym}(COO) and υ_{sym}(COO) stretching vibration bands to 1528–1580 and 1370–1420 cm^{-1}, respectively, in the complexes (Table 1). The $\Delta\upsilon$ (150–160 cm^{-1}) indicates the presence of monodentate carboxylate group [39].

The bands observed at 900–945 and 810–855 cm^{-1} can be assigned to coordinated water molecules [40].

New bands are found in the spectra of the complexes in the regions 530–552 and 400–500 cm^{-1} which can be assigned to υ(M–O) stretching vibrations of carbonyl oxygen and coordinated water attached to metal ions, respectively. It is noticed from the spectra of the parent LFX ligand and its metal complexes that some bands show significant wavenumber shifts in all complexes, although these groups did not participate in the bonding to metal ions. These bands are the υ(C=C), υ(C=N), υ(C–N), υ(C–F), υ(CH stretch in CH_3 and in CH_2 groups) and the benzene and pyridine rings stretching vibrations. These bands are either shifted to lower (9–60 cm^{-1}) or higher (6–25 cm^{-1}) frequencies. This shift is attributed to the change in the environment around these atoms as the results of coordination of LFX ligand to metal ions.

Therefore, it is concluded from the IR spectra that LFX behaves as neutral bidentate ligand coordinated to the metal ions via the carbonyl oxygen and protonated carboxylate oxygen in accordance with the previously published data on similar types of flouroquinolone drugs [23,24,37,38].

3.8. ^{1}H NMR spectral studies

Comparative study between the ^{1}H NMR data of LFX ligand and its zinc complex gives an idea about the ligatational behaviour of the ligand. The doublets at 7.89 and 7.87 ppm was assigned to the 5-H of LFX and Zn-LFX complex, respectively [23,24,37,38,41]. The bands at 8.93 and 8.91 ppm (s, H, CH of carbon 2) and 3.39 and 3.27 ppm (d, H, CH of carbon 3′) are assigned to the CH proton in the LFX ligand and Zn-LFX, respectively. While, the bands observed at 3.39 and 3.40 ppm (d, 4H, CH_2 of carbon 5′, 6′) and 3.55 and 3.37 ppm (d, 2H, CH_2 of carbon 2′) are assigned to the CH_2 protons in the LFX ligand and Zn-LFX complex, respectively. The bands observed at 1.46 and 1.48 ppm (d, 3H, CH_3 of carbon 1b) for LFX and Zn-LFX, respectively. In addition, bands observed at 1.44 ppm (d, 3H, CH_3 of carbon 3a') is found in both LFX and Zn-LFX. These bands are assigned to the CH proton in the LFX ligand and its Zn(II) complex. Upon comparison with the free LFX ligand, the signal observed at 13.5 ppm can be assigned to the carboxylate OH. This signal disappeared in the spectra of the complexes. Although the LFX ligand coordinated to the metal ions without proton displacement, the disappearance of this signal can be attributed to Zwitter-ion formation shown in Scheme 3 [41].

3.9. Electronic spectra and magnetic moments studies

A comparison of the electronic spectrum of the free LFX ligand with those of the corresponding metal complexes show some shifts that can be considered as evidence for the complex formation. Additionally the solid reflectance spectra of metal complexes show different bands at different wavelengths each one is corresponding to certain transition which suggests the geometry of the complexes. The magnetic moment values are listed in Suppl. Table 1. The diffused reflectance spectra of the complexes are dominated by intense intra-ligand charge transfer bands. The diffused reflectance spectrum of Cr(III) complex exhibits three bands at 27,855, 25,563, 13,441 cm^{-1} which may be assigned to the transitions $^4A_{2g}(F) \rightarrow {}^4T_{2g}(F)$, $^4A_{2g}(F) \rightarrow {}^4T_{2g}(F)$ and $^4A_{2g}(F) \rightarrow {}^4T_{2g}(P)$ spin allowed *d-d* transitions, respectively. The magnetic moment value is found to be 3.65 B.M which suggest an octahedral geometry [31,42,43]. The diffused reflectance spectrum of Mn(II) complex exhibit three bands at 25,189, 19,757, 16,570 cm^{-1}, which may be assigned to $^4T_{1g} \rightarrow {}^6A_{1g}$, $^4T_{2g}(G) \rightarrow {}^6A_{1g}$ and $^4T_{1g}(D) \rightarrow {}^6A_{1g}$ transitions, respectively, which suggests an octahedral geometry. The assignment of an octahedral geometry to the Mn(II) complex is further supported by its magnetic moment of 5.37 B.M [42,43]. From the diffused reflectance spectrum, it is observed that, the Fe(III) chelate exhibits a band at 21,522 cm^{-1}, which may be assigned to the $^6A_{1g} \rightarrow T_{2g}(G)$ transition in octahedral geometry [31,42]. The $^6A_{1g} \rightarrow {}^5T_1g$ transition appears to be split into two bands at 15,562 and 13,175 cm^{-1}. The Fe(III) complex is found to have magnetic moment value of 5.06 B.M., indicating octahedral geometry involving sp^3d^2 hybridization in Fe(III) ion [42,43]. The spectrum

shows also a band at 24,530 cm^{-1} which may be attributed to ligand to metal charge transfer. The diffused reflectance spectrum of the Co(II) complex gives three bands at 14,492, 15,099 and 22,031 cm^{-1}. The bands observed are assigned to the transitions $^4T_{1g}(F) \rightarrow {}^4T_{2g}(F)$ (ν_1), $^4T_{1g}(F) \rightarrow {}^4A_{2g}(F)$ (ν_2) and $^4T_{1g}(F) \rightarrow {}^4T_{1g}(P)$ (ν_3), respectively, suggesting an octahedral geometry around Co(II) ion [31,42–44]. The region at 28,585 cm^{-1} refers to the charge transfer band. The magnetic moment value is found to be 5.32 B.M. which is an indicative of octahedral geometry [42]. The Ni(II) complex reported herein is high spin with a room temperature magnetic moment value of 3.04 B.M. indicating that the Ni(II) complex is octahedral [31,43]. The diffused reflectance spectrum displays three bands at ν_1: 13,201 cm^{-1}: $^3A_{2g}(F) \rightarrow {}^3T_{2g}(F)$, ν_2: 14,804 cm^{-1}: $^3A_{2g}(F) \rightarrow {}^3T_{1g}$ (F) and ν_3: 20,243 cm^{-1}: $^3A_{2g}(F) \rightarrow {}^3T_{1g}$ (P) [31,42]. The spectrum shows also a band at 25,315 cm^{-1} which may be attributed to ligand to metal charge transfer.

The diffused reflectance spectrum of the Cu(II) chelate has two broad bands at 15,670 and 20,124 cm^{-1} which can be assigned to $^2Eg \rightarrow {}^2T_{2g}$ and $^2B_{1g} \rightarrow {}^2A_{1g}$ transitions characteristic of octahedral geometry [31,40–42]. The magnetic moment of this complex is 1.94 B.M. which fall within the range normally observed for octahedral Cu(II) complexes [31,42]. A moderately intense peak observed in the range of 24,764 cm^{-1} is due to ligand to metal charge transfer transition [31,42].

The Zn(II), UO_2(II) and Th(IV) complexes are diamagnetic. According to the empirical formulae, an octahedral geometry was proposed for these chelates.

3.10. Thermal analyses

Thermogravimetric studies (TG) for the complexes were carried out within the temperature range from room temperature up to 800 °C. TG results are in good agreement with the suggested formulae resulted from microanalyses data (Suppl. Table 1). The determined temperature ranges and percent mass losses of the solid complexes on heating are given in Table 2, which revealed the following findings:

The TG curve of LFX drug exhibits a first estimated mass loss of 45.02% (calcd. 44.98%) at 200–345 °C, which may be attributed to the liberation of $C_{10}H_{10}N_2$ molecule as gases (Table 2). The second estimated mass loss of 54.59% (calcd. 54.94%), at 345–620 °C, may be attributed to the liberation of $C_7H_9F_2NO_3$ molecule as gases.

The $[Fe(LFX)(H_2O)_4]Cl_3{\cdot}H_2O$ complex gives a decomposition pattern as follows; the first stage is one step within the temperature range of 30–120 °C, representing the loss of H_2O (hydrated) and Cl_2 gases with a found mass loss of 14.11% (calcd. 14.70%). The subsequent steps represent the loss of three coordinated water, HCl and LFX drug with a mass loss of 71.75% (calcd. 72.00%). At the end of the thermogram, the metal oxide Fe_2O_3 was the residue 12.33% (calcd. 13.30%), which is in good agreement with the calculated metal content obtained and the results of elemental analyses (Table 2).

The $[Ni(LFX)(H_2O)_4]Cl_2{\cdot}H_2O$ complex is thermally decomposed in four stages. The first stage corresponds to a mass loss of 2.67% (calcd. 3.15%) within the temperature range 30–130 °C and represents the loss of one molecule of hydrated water. The second stage corresponds to a mass loss of 12.68% (calcd. 12.90%) within the temperature range 130–250 °C and represents the loss of four coordinated water molecules. The third and fourth stages, 250–350 and 350–700 °C, with a found mass loss of 12.45% (calcd. 12.43%) and 59.74% (calcd. 58.69%), respectively, are reasonably accounted for the loss of Cl_2 and decomposition of the organic part of the complex leaving out NiO as a residue with a found mass loss of 11.88% (calcd. 13.13%).

Table 2
Thermoanalytical results (TG, DTG and DTA) of LFX and its metal complexes.

Complex	TG range (°C)	DTG_{max} (°C)	n^a	Estim (Calcd) %		Assignment	Metallic residue	DTA (°C)
				Mass loss	Total mass loss			
LFX	200–345	311	1	45.02 (44.98)		Loss of $C_{10}H_{10}N_2$	–	308(−), 329(−), 528(−)
	345–620	539	1	54.59 (54.94)	99.61 (99.92)	Loss of $C_7H_9F_2NO_3$		
$[Fe(LFX)(H_2O)_4]$	30–120	73	1	14.11 (14.70)		Loss of H_2O and Cl_2		78(+), 219(+), 300(−), 320(−), 410(−), 530(−)
$Cl_3{\cdot}H_2O$	120–270	212	1	13.80 (15.00)		Loss of HCl and $3H_2O$		
	270–650	321, 387, 527	3	57.95 (57.00)	87.67 (86.70)	Loss of $C_{17}H_{20}F_2N_3O_{2.5}$	½ Fe_2O_3	
$[Ni(LFX)(H_2O)_4]$	30–130	84	1	2.76 (3.15)		Loss of H_2O		207(+), 318(−), 460(+), 606(−)
	130–250	200	1	12.68 (12.60)		Loss of $4H_2O$	NiO	
$Cl_2{\cdot}H_2O$	250–350	316	1	12.45 (12.43)		Loss of Cl_2		
	350–700	595	1	59.74 (58.69)	88.12 (86.87)	Loss of $C_{17}H_{19}F_2N_3O_2$		
$[Cu(LFX)(H_2O)_4]$	30–95	53	1	5.68 (6.06)		Loss of $2H_2O$		213(+), 273(+), 307(−), 416(−), 479(−)
	95–220	209	1	12.16 (12.13)		Loss of $4H_2O$	CuO	
$Cl_2{\cdot}2H_2O$	220–310	296	1	11.59 (11.96)		Loss of Cl_2		
	310–525	411	1	56.15 (56.47)	85.58 (86.62)	Loss of $C_{17}H_{19}F_2N_3O_3$		
$[UO_2$ (LFX) $(H_2O)_2](NO_3)_2$	200–385	311	1	42.05 (41.97)		Loss of $2H_2O$, $2NO_3$ and $C_7H_{11}F_2N_2O_2$		303(−), 396(+), 229(−)
	385–690	534.37	1	10.86 (10.78)	52.91 (52.75)	Loss of $C_{10}H_8NO$	UO_2	

[a] Number of decomposition steps.

Table 3
Thermodynamic data of the thermal decomposition of metal complexes of LFX.

Complex	Decomp. Temp. (°C)	E^* (kJ mol^{-1})	A (s^{-1})	ΔS^* (kJ mol^{-1})	ΔH^* (kJmol^{-1})	ΔG^* (kJ mol^{-1})
LFX	200–345	17.408	5.57×10^3	−58.70	14.82	77.65
	345–620	52.289	7.49×10^6	−60.81	47.80	137.05
$[Fe(LFX)(H_2O)_4]Cl_3 \cdot H_2O$	30–120	2.29	1.25×10^6	−203.92	1.73	15.41
	120–270	27.35	1.07×10^7	−92.44	25.81	42.96
	270–650	14.62	2.57×10^6	−205.28	12.43	66.52
$[Ni(LFX)(H_2O)_4]Cl_2 \cdot H_2O$	30–130	24.33	6.35×10^4	−37.31	23.33	27.79
	130–250	48.62	1.09×10^{10}	−105.37	46.37	74.84
	250–350	78.19	3.54×10^{11}	−91.71	74.34	116.86
	350–700	59.67	2.9×10^5	−165.43	54.93	149.19
$[Cu(LFX)(H_2O)_4]Cl_2 \cdot 2H_2O$	30–95	4.59	8.21×10^4	−207.24	3.66	26.77
	95–221	15.70	1.92×10^7	−166.34	14.13	45.54
	221–310	20.15	8.54×10^6	−213.23	17.27	91.02
	310–523	52.29	1.46×10^5	−144.79	47.63	128.75
$[UO_2\ (LFX)\ (H_2O)_2] \cdot (NO_3)_2$	200–385	13.07	4.61×10^6	−209.51	11.03	62.54
	385–686	64.63	3.16×10^6	−103.38	61.03	105.81

The $[Cu(LFX)(H_2O)_4]Cl_2 \cdot 2H_2O$ complex is thermally decomposed in four stages. The first stage corresponds to a mass loss of 5.68% (calcd. 6.06%) within the temperature range 30–95 °C and represents the loss of two molecules of hydrated water. The second and third stages correspond to a mass loss of 12.16% (calcd. 12.13%) and 11.59% (11.96%) within the temperature range 95–220 and 220–310 °C and represent the loss of two coordinated water and Cl_2 gases, respectively. The last stage, 310–525 °C with a found mass loss of 56.15% (calcd. 56.47%), is reasonably accounted for the decomposition of the organic part of the complex leaving out CuO as a residue with a found mass loss of 14.42% (calcd. 13.38%).

$[UO_2(LFX)(H_2O)_2](NO_3)_2$ chelate exhibits two steps of decomposition within the temperature range 200–690 °C. In the first step of decomposition within the temperature range 200–385 °C in which two coordinated water molecules, $2NO_3$ and $C_7H_{11}F_2N_2O_2$ gases with an estimated mass loss of 42.05% (calcd. 41.97%) occurs. The second step within the temperature range 385–690 °C, involves liberation of $C_{10}H_8NO$ molecule with an estimated mass loss of 10.86% (calcd. 10.78%).

3.11. Kinetic data

The kinetic and thermodynamic parameters of thermal degradation process have been calculated using Coats–Redfern [45] and Horowitz–Metzger methods [46]. Coats–Redfern relation [45] is as follows:

$$\ln \frac{-\ln(1-\alpha)}{T^2} = \ln\left(\frac{AR}{\beta E}\right) - \left(\frac{E}{RT}\right) \tag{4}$$

where α represents the fraction of sample decomposed at time t, defined by: $\alpha = (w_o - w_t)/(w_o - w_\infty)$, w_o, w_t and w_∞ are the weight of the sample before the degradation, at temperature t and after total conversion, respectively. T is the derivative peak temperature. β is the heating rate = dT/dt, E and A are the activation energy and the Arrhenius pre-exponential factor, respectively. A plot of $\ln[-(\ln(1-\alpha))/T^2]$ versus $1/T$ gives a straight line whose slope (E/R) and the pre-exponential factor (A) can be determined from the intercept.

The Horowitz–Metzger equation [44] is an illustrative of the approximation methods. These authors derived the relation:

$$\log \frac{(1-(1-\alpha)^{1-n}}{1-n} = \frac{E\theta}{2.303RT_s^2}, \quad \text{for } n \neq 1 \tag{5}$$

when $n = 1$, the LHS of Eq. (5) would be $\log[-\log(1-\alpha)]$. For a first order kinetic process the Horowitz–Metzger equation may be written in the form (Eq. (6)):

$$\log\left[\log\left(\frac{w_\alpha}{w_\gamma}\right)\right] = \frac{E^*\theta}{2.303RT_s^2} - \log 2.303 \tag{6}$$

where $\theta = T - TS$, $w_\gamma = w_\alpha - w$, w_α = mass loss at the completion of the reaction; w = mass loss up to time t. The plot of $\log[\log(w_\alpha/w_\gamma)]$ versus θ was drawn and found to be linear from the slope of which E^* was calculated. The pre-exponential factor, A, was calculated from Eq. (7):

$$\frac{E^*}{RT_s^2} = \frac{A}{\varphi \exp(-E^*/RT_s)} \tag{7}$$

A number of pyrolysis processes can be represented as a first order reaction. The degradation of a series LFX complexes was suggested to be first order, therefore we assume $n = 1$ for the remainder of the present text. The other thermodynamic parameters such as activation energy (E), preexponential factor (A), entropy of activation (ΔS), enthalpy of activation (ΔH) and free energy of activation (ΔG) of decomposition steps were calculated using Coats–Redfern [45] and Horowitz–Metzger [46] methods and the average values obtained are listed in Table 3. From the results, the following remarks can be pointed out:

- The high values of the energy of activation of the complexes reveal the high stability of such chelates due to their covalent bond character [47].
- The positive sign of ΔG for the investigated complexes reveals that the free energy of the final residue is higher than that of the initial compound, and all the decomposition steps are non-spontaneous processes. Also, the values of the activation, ΔG increases significantly for the subsequent decomposition stages of a given complex. This is due to increasing the values of $T\Delta S$ significantly from one step to another which overrides the values of ΔH [47].
- The negative values of ΔS for all the complexes indicate more ordered activated complex than the reactants or the reaction is slow [47].

3.12. X-ray powder diffraction of complexes

X-ray powder diffraction pattern in the $0° < 2\theta < 60°$ of the LFX ligand and its metal complexes were carried out in order to give an insight about the lattice dynamics of these compounds. The X-ray powder diffraction obtained reflects a shadow on the fact that each solid represents a definite compound of a definite structure

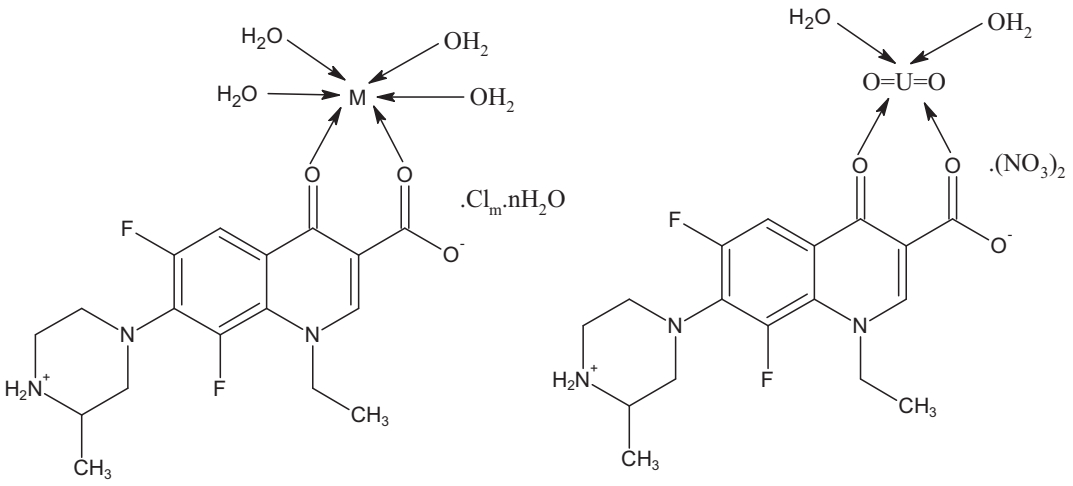

M = Cr(III), Mn(II), Fe(III), Co(II), Ni(II), Cu(II), Zn(II) and Th(IV)
m = 2-4, n = 0-2

Fig. 2. Structures of metal complexes.

which is not contaminated with starting materials. Such facts suggest that the LFX ligand and its Cr(III), Fe(III), Co(II), Ni(II), Cu(II) and Th(IV) complexes are crystalline while Mn(II), Zn(II) and UO_2(II) complexes are amorphous.

3.13. Structural interpretation

From all of the above observations, the structure of these complexes may be interpreted in accordance with complexes of LFX drug with a similar distribution of like coordinating sites [14,15,23,24]. The structural information from the previously reported complexes is in agreement with the data reported in this paper based on the p*K*, IR, molar conductance, magnetic and electronic spectra measurements. Consequently, the structures proposed are based on octahedral complexes. The LFX drug always coordinates via the carbonyl O and the protonated O atoms forming a two binding chelating sites. The proposed general structures are shown in Fig. 2.

3.14. Biological activity

3.14.1.1. Antimicrobial activity

The question about the involvement of metal ligand complexes in medical treatment are of special interest. To assess the biological potential of the synthesized compounds, the LFX ligand and its metal complexes was tested against the selected bacteria and fungi. The in vitro antibacterial and antifungal activity tests were performed using the disc diffusion method. Tetracycline and amphotricine were used as positive control for bacteria and fungus, respectively. The growth of inhibition zones after incubation is shown in Table 4. The synthesized compounds were found to possess remarkable bactericidal and fungicidal properties. It is however interesting that the biological activity gets enhanced on undergoing complexation with the metal ions.

From structure point of view of the prepared compounds with their effects on microbial tested, it is clear that formation of the chelate derivatives in 1:1 molar ratio (M:L) sometimes increase the biological activity as appeared from the results. So the enhanced activities of the metal complexes compared to the free ligand may be attributed to the increase in the number of oxygen group around the central metal atom arising from chelation in 1:1 molar ratio (M:L) and hence, the central metal atom was not only the responsible for biological activity because some metal complexes can enhance the activity and others can reduced this activity with respect to the parent ligand. Finally, to complete the evaluation of biological activity of the synthesized compounds, some comparison with the known standard antibiotics were performed and the data are summarized in Table 4 and shown in Fig. 3). Using *Staphy-*

Table 4
Biological activity of binary LFX-metal complexes.

Sample	Inhibition zone diameter (mm/mg sample)			
	E. coli	*Staphylococcus aureus*	*Aspergillus flavus*	*Candida albicans*
Control: DMSO	0.0	0.0	0.0	0.0
LFX	43	44	0.0	11
$[Cr(LFX)(H_2O)_4]\cdot Cl_3$	36	38	0.0	12
$[Mn(LFX)(H_2O)_4]\cdot Cl_2$	43	48	0.0	11
$[Fe(LFX)(H_2O)_4]Cl_3\cdot H_2O$	40	46	0.0	13
$[Co(LFX)(H_2O)_4]\cdot Cl_2$	40	44	0.0	20
$[Ni(LFX)(H_2O)_4]Cl_2\cdot H_2O$	40	40	0.0	21
$[Cu(LFX)(H_2O)_4]Cl_2\cdot 2H_2O$	42	43	0.0	12
$[Zn(LFX)(H_2O)_4]\cdot Cl_2$	42	47	0.0	12
$[Th(LFX)(H_2O)_4]\cdot Cl_4$	40	37	0.0	12
$[UO_2\ (LFX)\ (H_2O)_2]\cdot (NO_3)_2$	37	42	0.0	12
Standard				
Tetracycline	33	31	–	–
Amphotericin B	–	–	16	19

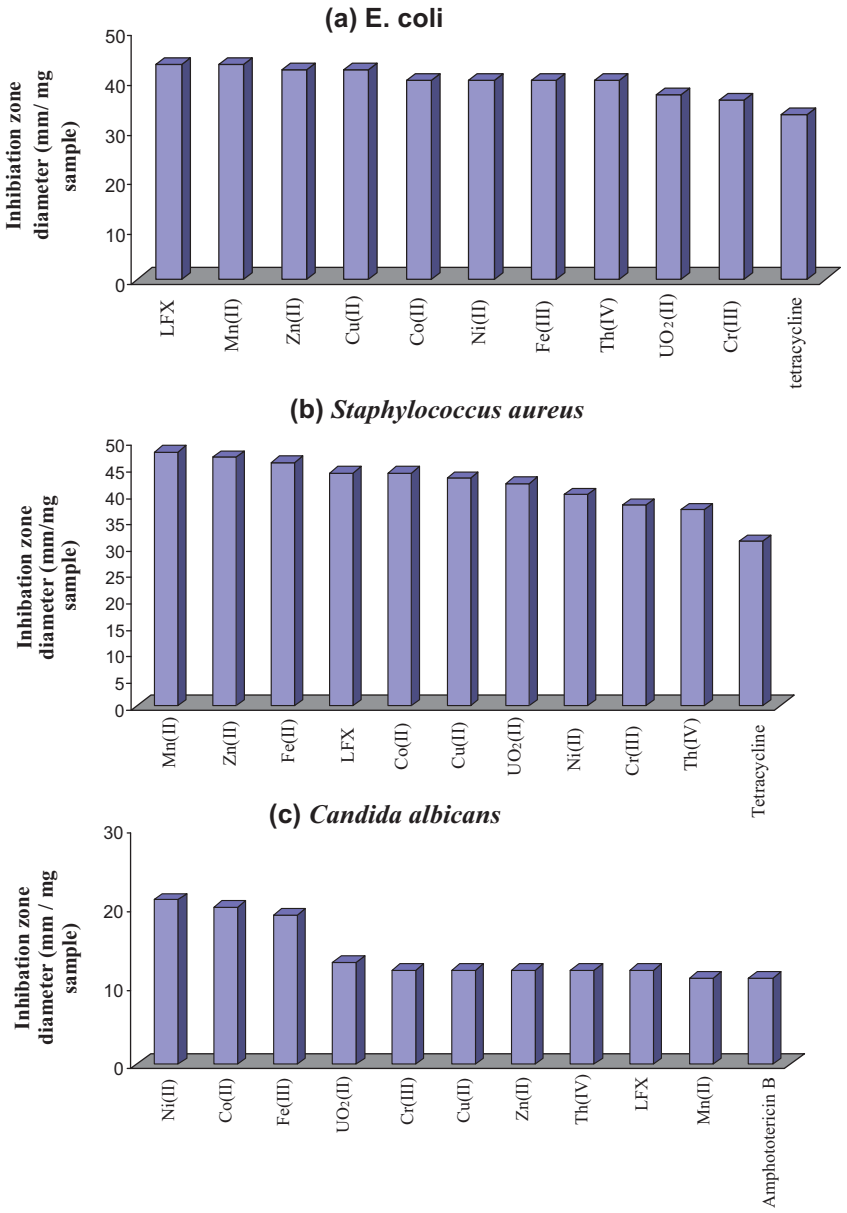

Fig. 3. Biological activity of LFX and its metal complexes.

lococcus aureus (G^+) and *Escherichia coli* bacteria (G^-), it is noticed that the biological activity of Fe(III), Mn(II) and Zn(II) complexes are higher than that of the LFX drug and tetracycline standard. In addition, the biological activity of Ni(II), Cu(II), Cr(III), UO_2(II) and Th(IV) complexes are lower than that of the free LFX ligand. For Co(II) complex, its biological activity is the same like that of LFX. Using *Candida albicans* fungus, the biological activity of the metal complexes are found to be higher than that of the free LFX ligand but lower than amphotricine standard except Co(II) and Ni(II) complexes.

The LFX drug presented here and its transition metal complexes gave better results against the growth of bacteria and fungi. It is found that the activity increases upon co-ordination. The increased activity of the metal chelates can be explained on the basis of

Table 5
Antibreastic cancer activity of LFX and its binary complexes.

Complex	Surviving fraction (MCF7)					IC50 (μg/ml)
	Concentration (μg/ml)					
	0.0	5	12.5	25	50	
LFX	1.00	0.64	0.53	0.27	0.19	14.0
$[Mn(LFX)(H_2O)_4]\cdot Cl_2$	1.00	0.99	0.99	0.95	0.89	–
$[Co(LFX)(H_2O)_4]\cdot Cl_2$	1.00	0.64	0.47	0.28	0.22	11.2
$[Ni(LFX)(H_2O)_4]Cl_2\cdot H_2O$	1.00	0.99	1.03	1.05	0.95	–
$[Cu(LFX)(H_2O)_4]Cl_2\cdot 2H_2O$	1.00	0.89	0.89	0.90	0.59	–
$[Zn(LFX)(H_2O)_4]\cdot Cl_2$	1.00	0.99	0.89	0.75	0.40	43.1

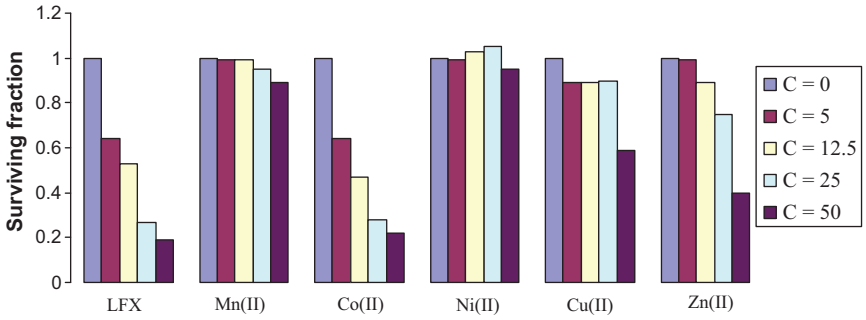

Fig. 4. The anticancer activity of LFX and its binary complexes.

chelation theory [48]. The orbital of each metal ion is made so as to overlap with the ligand orbital. Increased activity enhances the lipophilicity of complexes due to delocalization of pi-electrons in the chelate ring [46]. In some cases increased lipophilicity leads to breakdown of the permeability barrier of the cell [44,48,49].

3.14.1.2. Cytotoxic activity

The LFX drug and its metal complexes were tested for their activity against breast cancer cell line (MCF7) by using 100 μg/ml concentration. From these result summarized in Table 5), it is clear that LFX, $[Mn(LFX)(H_2O)_4]\cdot Cl_2$, $[Co(LFX)(H_2O)_4]\cdot Cl_2$, $[Ni(LFX)(H_2O)_4]Cl_2\cdot H_2O$, $[Cu(LFX)(H_2O)_4]Cl_2\cdot 2H_2O$ and $[Zn(LFX)(H_2O)_4]\cdot Cl_2$ were found to be very active against breast cancer cells with inhibition ratio values between 70–85.5%, while other complexes utilized in this work had been shown to be inactive (less than 70% inhibition). The pattern of activity can be determined using different drug concentrations (Table 5). LFX, $[Co(LFX)(H_2O)_4]\cdot Cl_2$ and $[Zn(LFX)(H_2O)_4]\cdot Cl_2$ were found to be very active with IC50 values 14, 11.2 and 43.1, respectively, while other complexes are found to be inactive at lower concentration than 100 μg/ml (Fig. 4).

4. Conclusion

In the present paper, the data obtained from elemental analysis, FT-IR, electronic absorption spectra, thermal analyses, molar conductivities and magnetic susceptibility measurements show that the complexes of Cr(III), Mn(II), Fe(III), Co(II), Ni(II), Cu(II), Zn(II), UO_2(II) and Th(IV) metal ions with the investigated LFX drug may be formulated, where bonding in 1:1 complexes are formed through coordination with oxygen of the carbonyl group and protonated carboxylic O group. The complexes obtained contain water of coordination in their sphere. The investigated LFX drug acts as neutral bidentate ligand. The solid complexes prepared behave as electrolytes in DMF solution. The diffused reflectance spectra of the investigated complexes together with the magnetic moment measurements support the octahedral geometry. The complexes also exhibit M to L charge transfer spectra. The bands observed at higher wavenumbers which are not observed in the spectrum of the free LFX ligand may be ascribed to d–d electronic transition within the metal ions.

The dissociation constants of lomefloxacin and stability constants of its binary complexes have been determined spectrophotometrically in aqueous solution at 25 ± 1 °C and at 0.1 M KNO_3 ionic strength. Calculation of formation constants has evidenced its strong affinity towards metal cations. Also, the % metal ion content (Suppl. Table 1) as well as the TG data (Table 2) are concordant with the mononuclear structure (Fig. 2). From the interpretation of elemental and thermal analyses and spectral studies as well as magnetic susceptibility and molar conductivity measurements, it is possible to draw up the proposed structures of the complexes as shown in Fig. 2. The in vitro antibacterial and antifungal activity tests were performed using the disc diffusion method. Also the anticancer activity against breast cancer cell line (MCF7) was also studied. The complexes show a remarkable biological and anticancer activity.

Appendix A. Supplementary data

Supplementary data associated with this article can be found, in the online version, at doi:10.1016/j.saa.2011.05.089.

References

[1] www.drugbank.ca.
[2] I. Turel, Coord. Chem. Rev 232 (2002) 27–47.
[3] Y. Xia, Z.Y. Yang, S.L. Morrisnatschke, K.H. Lee, Curr. Med. Chem 6 (1999) 179–194.
[4] A.D. da Silva, M.V. de Almeida, M.V.N. de Souza, M.R.C. Couri, Curr. Med. Chem. 10 (2003) 21–39.
[5] M.V.N. de Souza, Mini-Rev. Med. Chem. 5 (2005) 1009–1017.
[6] G. Anquetin, J. Greiner, N. Mahmoud, M.S. Hayat, R. Gozalbes, K. Farhati, F. Derouin, A. Aubry, E. Cambau, P. Vierling, Eur. J. Med. Chem. 41 (2006) 1478–1493.
[7] M. Ruiz, R. Ortiz, L. Perello, S. Garcıa-Granda, M.R. Dıaz, Inorg. Chim. Acta 217 (1994) 149–154.
[8] M. Ruiz, L. Perello, J. Server-Carrio, R. Ortiz, S. Garcıa-Granda, M.R. Diaz, E. Canton, J. Inorg. Biochem. 69 (1998) 231–239.
[9] B. Macias, M.V. Villa, M. Sastre, A. Castineiras, J. Borras. J. Pharm. Sci. 91 (2002) 2416–2423.
[10] Z.H. Chohan, C.T. Supuran, A. Scozzafava, J. Enzyme Inhib. Med. Chem. 20 (2005) 303–307.
[11] Z.H. Chohan, H. Pervez, A. Rauf, C.T. Supuran, Met. Based Drugs 8 (2001) 263–267.
[12] M.P. Lopez-Gresa, R. Ortiz, L. Perello, J. Latorre, M. Liu-Gonzalez, S. Garcıa-Granda, M. Perez-Priede, E. Canton, J. Inorg. Biochem. 92 (2002) 65–74.
[13] J.R. Anacona, C. Toledo, Trans. Met. Chem. 26 (2001) 228–231.
[14] I. Turel, L. Golic, P. Bukovec, M. Gubina, J. Inorg. Biochem. 71 (1998) 53–60.
[15] I. Turel, I. Leban, N. Bukovec, J. Inorg. Biochem. 66 (1997) 241–245.
[16] F. Gao, P. Yang, J. Xie, H. Wang, J. Inorg. Biochem. 60 (1995) 61–67.
[17] S. Jain, N.K. Jain, K.S. Pitre, J. Pharm. Biomed. Anal. 29 (2002) 795–801.
[18] D.K. Saha, S. Padhye, C.E. Anson, A.K. Powell, Inorg. Chem. Commun. 5 (2002) 1022–1027.
[19] H. Beraldo, D. Gambino, Mini Rev. Med. Chem. 4 (2004) 31–39.
[20] C. Chulvi, M.C. Munoz, L. Perello, R. Ortiz, M.I. Arriortua, J. Via, K. Urtiaga, J.M. Amigo, L.E. Ochando, J. Inorg. Biochem. 42 (1991) 133–138.
[21] M. Ruiz, R. Ortiz, L. Perelloĭ, A. Castiñ eiras, M. Quiroĭs, Inorg. Chim. Acta 211 (1993) 133–139.
[22] Z.F. Chen, R.G. Xiong, J. Zhang, X.T. Chen, Z.L. Xue, X.Z. You, Inorg. Chem. 40 (2001) 4075.
[23] M.S. Refat, G.G. Mohamed, R.F. de Farias, A.K. Powell, M.S. El-Garib, S.A. El-Korashy, M.A. Hussien, J. Therm. Anal. Calor. 102 (2010) 225–232.
[24] M.S. Refat, G.G. Mohamed, J. Chem. Eng. Data 55 (2010) 3239–3246.
[25] I.M. Issa, R.M. Issa, M.R. Mahmoud, Y.M.Z. Temerk, Physik. Chem. 254 (1973) 314–318.
[26] I. Sakiyan, E. Logoglu, S. Arslan, N. Sari, Bio. Met. 17 (2004) 115–120.
[27] P. Skehan, R. Storeng, J. Natl. Cancer Inst. 42 (1990) 1107–1112.
[28] M.M. Abd-Elzaher, J. Chin. Chem. Soc. 48 (2001) 153–158.
[29] D.S. Lee, H.J. Han, K. Kim, W.B. Park, J.K. Cho, J.H. Kim, J. Pharm. Biomed. Anal. 12 (1994) 157–164.
[30] J. Sulkowsha, R. Staroscik, Pharmazie 30 (1975) 405–408.
[31] G.G. Mohamed, N.E.A. El-Gamel, Spectrochim. Acta A 60 (2004) 3141–3154.
[32] A.D. Taneja, K.P. Srivastova, J. Inorg. Nucl. Chem. 33 (1971) 2678–2680.
[33] R.G. Anderson, G. Nickless, Anal. Chim. Acta 39 (1967) 469–477.
[34] (a) H. Irving, R.J.P. Williams, Nature 162 (1948) 746–747;
(b) H. Irving, R.J.P. Williams, J. Chem. Soc. (1953) 3192–3210.

[35] G.H. Olie, S. Olive, The Chemistry of the Catalyzes Hydrogenation of Carbon monoxide, Springer, Berlin, 1984.
[36] L.E. Orgel, An Introduction to transition Metal Chemistry Ligand Field Theory, 55, Methuen, 1966.
[37] L.M.M. Vieira, M.V. de Almeida, M.C.S. Lourenço, F.A.F.M. Bezerra, A.P.S. Fontes, Eur. J. Med. Chem. 44 (2009) 4107–4111.
[38] V.L. Dorofeev, Chem. Acta 38 (2004) 45–49.
[39] G.B. Deacon, R.J. Phillips, Coord. Chem. Rev. 33 (1980) 227–250.
[40] Z.M. Zaki, G.G. Mohamed, Spectrochim. Acta A 56 (2000) 1245–1250.
[41] S. Kumar, A. Rai, S.B. Rai, D.K. Rai, A.N. Singh, V.B. Singh, J. Mol. Str. 791 (2006) 23–29.
[42] M. Sakai, A. Hara, A. Anjo, M. Nakamura, J. Pharm. Biomed. Anal. 18 (1999) 1057–1067.
[43] F.A. Cotton, G. Wilkinson, C.A. Murillo, M. Bochmann, Advanced Inorganic Chemistry, 6th ed., Wiley, New York, 1999.
[44] H.F. Abd El-halim, M.M. Omar, G.G. Mohamed, Spectrochim. Acta A 78 (2011) 36–44.
[45] A.W. Coats, J.P. Redfern, Nature 201 (1964) 68–79.
[46] H.W. Horowitz, G.M. Jetzger, Anal. Chem. 35 (1963) 1464–1468.
[47] A. Ola, El-Gammal, Spectrochim. Acta A 75 (2010) 533–542.
[48] G.G. Mohamed, M.H. Soliman, Spectrochim. Acta A 76 (2010) 341–347.
[49] A.N.M.A. Alaghaz, R.A. Ammar, Eur. J. Med. Chem. 45 (2010) 1314–1322.